The Astrophysical Journal, 727:40 (16pp), 2011 January 20 doi:10.1088/0004-637X/727/1/40
© 2011. The American Astronomical Society. All rights reserved. Printed in the U.S.A.

DEEP 21 cm H I OBSERVATIONS AT $z \approx 0.1$: THE PRECURSOR TO THE ARECIBO ULTRA DEEP SURVEY*

Wolfram Freudling[1], Lister Staveley-Smith[2], Barbara Catinella[3], Robert Minchin[4], Mark Calabretta[5], Emmanuel Momjian[6], Martin Zwaan[1], Martin Meyer[2], and Karen O'Neil[7]
[1] European Southern Observatory, Karl-Schwarzschild-Str. 2, 85748 Garching, Germany
[2] International Centre for Radio Astronomy Research M468, The University of Western Australia, Crawley, 6009, Australia
[3] Max-Planck-Institut für Astrophysik, Karl-Schwarzschild-Str. 1, 85748 Garching, Germany
[4] Arecibo Observatory, HC03 Box 53995, Arecibo, PR 00612, USA
[5] Australia Telescope National Facility, P.O. Box 76 Epping NSW 1710, Australia
[6] National Radio Astronomy Observatory, P.O. Box O, Socorro, NM, 87801, USA
[7] National Radio Astronomy Observatory, P.O. Box 2, Green Bank, WV 24944, USA
Received 2010 February 15; accepted 2010 November 2; published 2010 December 30

ABSTRACT

The "ALFA Ultra Deep Survey" (AUDS) is an ongoing 21 cm spectral survey with the Arecibo 305 m telescope. AUDS will be the most sensitive blind survey undertaken with Arecibo's 300 MHz Mock spectrometer. The survey searches for 21 cm H I line emission at redshifts between 0 and 0.16. The main goals of the survey are to investigate the H I content and probe the evolution of H I gas within that redshift region. In this paper, we report on a set of precursor observations with a total integration time of 53 hr. The survey detected a total of eighteen 21 cm emission lines at redshifts between 0.07 and 0.15 in a region centered around $\alpha_{2000} \approx 0^{\rm h}$, $\delta \approx 15^\circ 42'$. The rate of detection is consistent with the one expected from the local H I mass function. The derived relative H I density at the median redshift of the survey is $\rho_{\rm H\,I}[z = 0.125] = (1.0 \pm 0.3)\rho_0$, where ρ_0 is the H I density at zero redshift.

Key words: cosmology: observations – galaxies: evolution – radio lines: galaxies

Online-only material: color figures

1. INTRODUCTION

1.1. Neutral Hydrogen Surveys of the Local Universe

Large-area blind H I surveys have come of age since the first 21 cm multibeam receiver was installed at Parkes Observatory in 1997, to be followed by similarly powerful receiving systems at the Lovell telescope, the Arecibo telescope and the Effelsberg telescope. These surveys have allowed extensive areas of sky to be mapped for extragalactic neutral hydrogen, resulting in the detection of over 10^4 galaxies (Meyer et al. 2004; Wong et al 2006; Giovanelli et al. 2005; Winkel et al. 2008). Surveys that specifically targeted the zone of avoidance expanded the sky coverage even further (e.g., Rivers et al. 1999; Henning et al. 2000, 2010). Prior to this, the most extensive neutral hydrogen surveys were those carried out with the single-beam or dual-beam systems at Arecibo: the Arecibo H I Strip Survey (AHISS; Zwaan et al. 1997) the Arecibo Slice (Spitzak & Schneider 1998), and the Arecibo Dual Beam Survey (ADBS; Rosenberg & Schneider 2000). These were all limited by the available bandpass to maximum recessional velocities of around 8000 km s^{-1} ($z \simeq 0.03$) and had relatively slow mapping speeds compared to the more recent multibeam surveys.

Multibeam surveys have adopted the strategy of going wide rather than deep, since this generally results in the largest observed volume and the greatest number of detected objects. If a survey in the local universe is carried out with an integration time of 1 unit, then extending it to t units by making it wider will increase the volume covered by a factor of t, while extending it with a longer integration in the same area will increase the volume by a factor of $t^{3/4}$, if not limited by receiver bandwidth and the changing beam size with frequency is neglected. Going very deep is generally only advantageous if it becomes possible to reach a new population of galaxies, e.g., outside the local region, or galaxies at an earlier epoch in their evolution. Therefore, most survey time at Parkes and Lovell was spent on the relatively shallow H I Parkes All Sky Survey (Meyer et al. 2004, HIPASS) and the H I Jodrell All Sky Survey (Lang et al. 2003, HIJASS), respectively. These surveys were limited by sensitivity (as well as the available bandpass) to maximum recessional velocities of less than 14,000 km s^{-1} ($z \simeq 0.04$), even for the most massive systems. The deepest field survey carried out with the Parkes system (Minchin et al. 2003, HIDEEP) reached a noise level of only 3.2 mJy (at a velocity resolution of 18 km s^{-1}), considerably higher than AHISS (0.75 mJy at 18 km s^{-1}). The most sensitive H I surveys in the local universe are those pointed toward the CVn group (Kovač et al. 2009) and the Virgo cluster (Popping & Braun 2007).

Observational programs on the newer Arecibo *L*-band Feed Array (ALFA) system at Arecibo have followed a similar pattern with the largest surveys being devoted to large areas of sky. The Arecibo Legacy Fast ALFA Survey (Giovanelli et al. 2005, 2007, ALFALFA) is covering 7000 deg^2 to a noise level of 2.2 mJy (at 10 km s^{-1}) and the Arecibo Galaxy Environment Survey (Auld et al. 2006, AGES) is covering 200 deg^2 to a noise level of 0.75 mJy (at 10 km s^{-1}).

1.2. H I Observations Above $z = 0.1$

Currently, the Cornell H I digital archive (Springob et al. 2005), a homogeneous database of pointed H I observations of about 9000 optically selected galaxies, includes only a few objects with recessional velocities larger than 20,000 km s^{-1}. Even the ongoing ALFALFA and AGES surveys mentioned above only reach maximum recessional velocities of 18,000 and 20,000 km s^{-1}, respectively. However, in spite of challenges such as limited sensitivity and radio-frequency interference (RFI), some progress in the detection of H I emission from galaxies at redshifts beyond $z \sim 0.1$ has been made with

* The Arecibo Observatory is part of the National Astronomy and Ionosphere Center which is operated by Cornell University under a Cooperative Agreement with the National Science Foundation.

Table 1
H I Survey at $z > 0.1$

Reference	$a \times b$ ($'' \times ''$)	rms (mJy)	Δv (km s^{-1})	$z_{\rm min}$–$z_{\rm max}$	Ω_s ($\square$deg)	$n_{\rm det}$	Target
Zwaan et al. (2001)	18 × 20	0.11	39	0.17–0.19	0.4	1	A2218
Verheijen et al. (2007)	17 × 27	0.068	20	0.164–0.224	0.81	42	A963, A2192
Catinella et al. (2008)	230 × 270	0.11	27	0.17–0.245	...	≈30	Targeted emission line galaxies
Lah et al. (2007)	2.9 × 2.9	0.13	33	0.218–0.253	...	0[a]	Emission line galaxies in field around Quasar SDSSp J104433-012502
Lah et al. (2009)	3.3 × 3.3	0.16	36	0.33–0.40	...	0[a]	Galaxies in A370 field
AUDS precursor	200 × 200	0.08	5.2	0.07–0.16	0.09[b]	18	Field around 4 emission line galaxies
AUDS	200 × 200	0.05[c]	5.2	0–0.16	0.35	>200[c]	Random pointings

Notes. The columns are as follows: $a \times b$: beam size, rms: sensitivity of survey, Δv: channel width, $z_{\rm min} - z_{\rm max}$: redshift range, Ω_s: survey area given unless individual galaxies were targeted, $n_{\rm det}$: the number of detected H I lines.
[a] H I detected in stacked spectra.
[b] Only a small fraction of the survey area reached the listed rms sensitivity.
[c] Expected numbers based on extrapolation of the precursor data.

deep integrations of galaxy clusters with the Westerbork Synthesis Radio Telescope (Zwaan et al. 2001; Verheijen et al. 2007), pointed Arecibo observations of Hα-emitting galaxies (Catinella et al. 2008), and "stacked" Giant Metrewave Radio Telescope (GMRT) integrations of fields with existing redshift information (Lah et al. 2007, 2009). The parameters of these surveys are summarized in Table 1. These observations have shown that it is possible to study the gaseous properties of galaxies in environments different to the local universe, and at look-back times of up to 2–4 Gyr. Nevertheless, selection effects, limited sensitivity, and cosmic variance all conspire to make it challenging to obtain the accurate measurements required to quantify systematic evolutionary and environmental trends.

1.3. Evolution of the Gas Content of the Universe

The rate of conversion of gas into stars is one of the fundamental quantities that describe the evolution of galaxies and remains a difficult measurement to make for all but the most nearby galaxy populations (e.g., Madau et al. 1996; Haarsma et al. 2000; Bouwens et al. 2004; Wong 2009). At redshifts between zero and unity, the global comoving star formation rate appears to increase by a factor of five (Hopkins 2004). Molecular gas content also possibly increases over this redshift range (Daddi et al. 2008).

Early models of the evolution of cold gas predicted a constant conversion factor between gas supply and star formation and therefore led to a similar strong evolution of the cold gas content (Pei et al. 1999). Observations of local galaxies suggest that both hot and cold gas accretion significantly contribute to replenish the gas content of galaxies (see, e.g., the review by Sancisi et al. 2008), and the balance between the two might depend on redshift. The modern picture of a self-regulated equilibrium between the net inflow of gas and star formation leads to predictions of somewhat smaller evolution of the cold gas content at redshifts lower than two (Obreschkow & Rawlings 2009; Power et al. 2009). This appears to fit observations of damped Lyα systems (DLAs; e.g., Rao et al. 2005; Storrie-Lombardi & Wolfe 2000; Prochaska et al. 2004, 2005) which suggest that the redshift density of absorbers with $N_{\rm H} > 2 \times 10^{20}$ cm^{-2} increases only mildly, $dN_{\rm DLA}/dz = 0.05(1+z)^{1.1}$, which is consistent with constant comoving gas density.

Conversion from DLA measurements to a cosmic gas density $\Omega_{\rm H\,I}$ is unfortunately fraught with uncertainty, largely due to the small number of observed systems, but also due to uncertain systematic effects such as lensing and covering factor. Better measurements of the gas mass density from intermediate redshift DLAs are presently not possible because of the limited availability of space-based UV instruments. Rosenberg & Schneider (2003), Ryan-Weber et al. (2003), and Zwaan et al. (2005) compared local H I observations with the DLA number and argue that the number of galaxies found in their "blind" H I surveys is consistent with the number densities of DLAs at redshifts out to $z \approx 1.5$.

Unfortunately, direct measurement of the H I in emission at high redshift is difficult. Bridging the gap between 21 cm surveys at $z \sim 0$ and DLA surveys at high z, for example, to measure the cosmic H I mass density, requires deeper and more extensive surveys in the 21 cm line than currently available. To be useful, such measurements ideally need to (1) have better accuracy than existing measurements, (2) preferably not be tied to "biased" optical samples or galaxy overdensities, (3) be over a large enough cosmic volume that cosmic variance is not a limitation, (4) be at a significant redshift or look-back time, and (5) sample the H I mass function below the "knee" where the bulk of the gas may be locked up. Unfortunately, achieving all of the above probably awaits the Square Kilometre Array. However, many of the above goals can be partially achieved with a deep survey of a small field with the ALFA instrument on the Arecibo telescope. Such a survey is currently in progress at Arecibo. This "Arecibo Ultra Deep Survey" (AUDS) is the deepest blind survey ever carried out with the Arecibo telescope, the world's largest single dish radio telescope. The full survey should allow the accurate measurements of the H I mass function up to the redshift limit of ALFA of $z \approx 0.16$, corresponding to a look-back time of about 2 Gyr or roughly 25% of the time between $z \approx 1$ and $z \approx 0$. In this paper, we report on a precursor project for AUDS which tested our ability to achieve the very low noise levels required by the full survey.

2. ARECIBO ULTRA DEEP PRECURSOR SURVEY

2.1. Motivation

The goal of the AUDS is to carry out a blind 21 cm line survey at the highest redshift possible using the ALFA. A fundamental

requirement for the survey is the ability to survey a large volume to the highest practical redshift, which is given by the bandpass of the ALFA receiver and is about $z \approx 0.16$. Sampling galaxies that contribute most of the gas mass to the H I mass function at $z \approx 0$ requires sufficient sensitivity to detect some galaxies in the flat part of the luminosity function, i.e., galaxies down to at least $10^9\ M_\odot$.

With a line width of 200 km s^{-1}, a galaxy with $M_{\rm H\,I} = 10^{9.5}\ M_\odot$ has an integrated flux of 0.03 Jy km s^{-1} and a mean flux density of only 140 μJy at the far end of our redshift range. A sensitivity of 50 μJy is necessary to detect such a galaxy with at least 3σ significance per channel. AUDS will use a total of 1200 hr of observing time to survey a total area of 1/3 deg^2 with such a sensitivity. The integration time per pointing will be about 40 hr. This will be the longest integration time per pointing of any 21 cm survey ever conducted with the Arecibo telescope.

Before committing this large amount of observing time, we carried out precursor observations to test the feasibility of extremely deep surveys with the Arecibo telescope. These precursor observations were carried out from 2004 October to 2005 February. The maximum redshift at which H I line emission can be probed by AUDS is $z = 0.16$ and is set by the ALFA multibeam receiver, which operates in the 1225–1525 MHz frequency range. However, the lower end of such an interval (i.e., frequencies below 1270 MHz, or $z > 0.12$) is heavily affected by RFI. Thus, we carefully chose a suitable target field with previously measured optical redshifts that would guarantee a few H I detections across the whole redshift range and that would allow us to test our algorithms of signal extraction in the presence of strong RFI. Note that for this precursor survey an interim back end with a total bandwidth of 100 MHz was used. The redshift range from $z = 0$ to 0.07, which will be sampled by the full survey, was therefore not accessible by the precursor survey.

2.2. Mapping Strategy

To reach the deepest possible observations with the multibeam array ALFA, we used a "drift and chase" mode to cover the survey region in a uniform manner. For that purpose, we rotated the feed array to an orientation so that a single position on the sky drifts through the three central beams. The basic strategy was to point 10 arcmin ahead of the target field with the central beam, and then let the sky drift past for 100 s of time (or 20 arcmin). Subsequently, the telescope drove back to the starting point and the whole procedure was repeated. The feed array remained stationary during each drift, and rotated to track the sky only between drifts. This strategy is ideal for Arecibo because of its sensitivity to ground spillover. Keeping the orientation and therefore the spillover constant during each drift results in the best possible baselines. At the same time, the "on" and "off" source integration are as close as possible in time and allow removal of temporal changes in receiver gain and interference.

An additional advantage of drift scanning is that positions and fluxes of sources can be measured at the full telescope resolution at least in the scanning direction. The goal of the full AUDS will be to obtain fully sampled two-dimensional maps. This is achieved by introducing offsets of about 1/10th of the beam width between the individual drifts. However, to reach the highest possible sensitivity for the precursor observations, we repeated all our scans at exactly the same declination. The resultant sky coverage therefore consists of three disjoint strips, each of length 1500 arcsec. This footprint is shown in Figure 1. Only a small part of the central strip is covered by three beams in each of the scans.

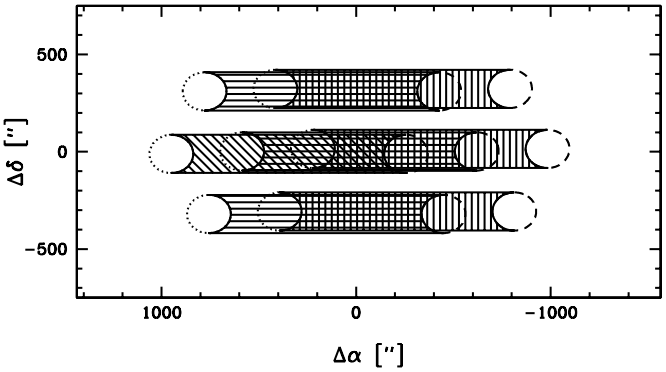


Figure 1. Footprint of the AUDS precursor survey. Dashed circles are the positions of the seven ALFA beams at the start of a scan, and the dotted line at the end of a scan. The central strip is covered by three beams, whereas the outer two strips are covered by only two beams.

2.3. Target Selection

As explained in the previous section, the deepest part of the survey was a strip with the extension in declination given by the size of the ALFA beams, and about 13 arcmin long in right ascension. To make the precursor observations a useful test of our ability to detect galaxies, we have used the Sloan Digital Sky Survey (SDSS) DR2 (Abazajian et al. 2004) spectroscopic database to identify a target field with the following characteristics: (1) observable from Arecibo during night time; (2) including at least one H I-rich galaxy in the redshift range $0.09 \leqslant z \leqslant 0.12$, corresponding to the relatively RFI-free 1270–1300 MHz frequency window; (3) including at least one H I-rich galaxy at lower redshift; and (4) not contaminated by strong radio continuum sources. In practice, we generated a list of good candidates for H I detection in the highest redshift end of our survey, and visually inspected the SDSS images, looking for the presence of additional disk galaxies within a few arcminutes from the main target. The selection criteria for *good* H I candidates are similar to those successfully used by Catinella et al. (2008) to identify H I-rich galaxies at intermediate redshifts ($z > 0.16$) detectable with Arecibo. Basically, we looked for relatively isolated, non-interacting galaxies with disk morphology, presence of Hα line emission, late-type spectra, and redshift as close as possible to our limit, $z = 0.16$.

The field selected for our precursor observations is shown in Figure 2. There are a total of 31 galaxies with measured redshift listed in the SDSS DR7 (Abazajian et al. 2009). Two of them are in the foreground of our survey at $z < 0.07$, 17 of them within our redshift range $0.07 < z < 0.15$, and 14 in the background at $z > 0.15$. There are more than 1000 additional SDSS galaxies in the field without optical redshifts. The field includes several late-type galaxies at different redshifts. Some of them are at or close to frequencies which are affected by RFI for a large fraction of the time.

2.4. Observations and Data Reduction

We used the Wideband Arecibo Pulsar Processors (WAPPs) with 100 MHz bandwidth and 4096 channels (three-level sampling). This resulted in a channel separation of 24.4 kHz (5.2 km s^{-1} at $z = 0$). For this experiment, the WAPPs were

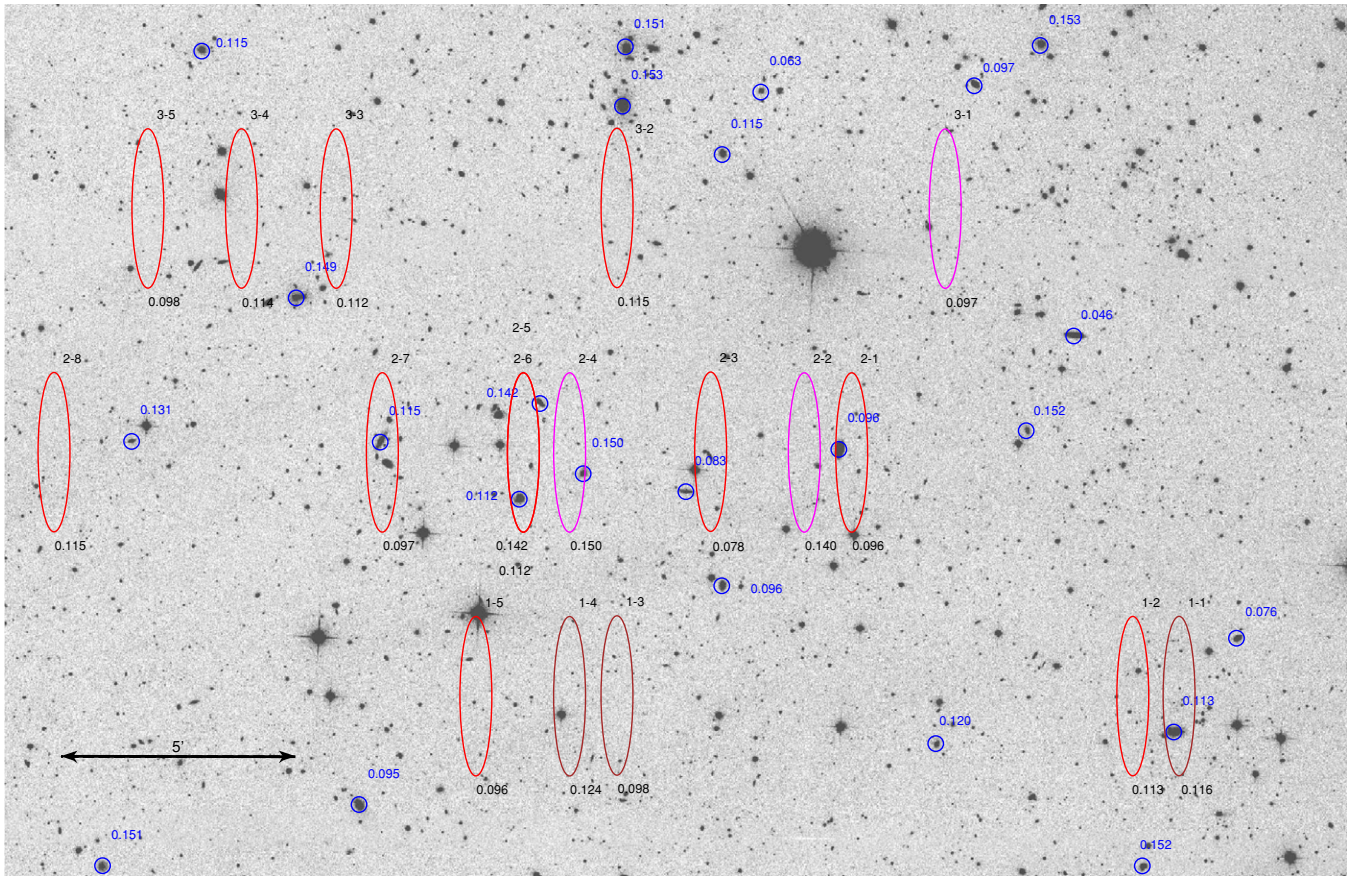


Figure 2. SDSS *r*-band image of the AUDS precursor field. H I detections are marked with the expected uncertainty in position for high signal-to-noise detections. The colors of the ellipses code the quality of the detections, red for the best quality ($q = 1$), brown for medium quality ($q = 2$), and magenta for low quality spectra ($q = 3$). Galaxies with available SDSS redshifts are marked as circles with their redshift. Note that H I can be detected at any position within the shown region, and that low signal-to-noise detections have much larger positional uncertainties (see the text).

(A color version of this figure is available in the online journal.)

tuned to a central frequency of 1275 MHz, giving coverage over the range 1325–1225 MHz (corresponding to $z = 0.07$–0.16).

We spent a total of 53 1 hr sessions testing our "drift-and-chase" procedure on this target field. In the most sensitive part of the survey, the accumulated integration time per pointing was about 14 hr. The total telescope time spent to carry out these observations was about 50% higher than the actual time spent on the drift scans. A significant fraction of these overheads were due to time losses at the start of each observing session and before and after each drift scan. For the full AUDS survey, overheads are expected to be about 25% since individual strips are longer.

The measured rms in the spectra of the most sensitive part of the precursor survey is about 80 μJy per 24.4 kHz channel throughout the bandpass, see Figure 3. This is close to the expectations based on the system temperature of 28 K, gain of 9 K Jy^{-1}, and the accumulated integration time per pointing of 14 hr. In Figure 4, we show the measured rms as a function of integration time at a frequency of 1270 MHz. It can be seen that the rms noise of the averaged spectra declined as $\sigma \propto \sqrt{1/t_{\rm int}}$ down to the longest achieved integration time.

Data reduction was performed using the *Livedata* and *Gridzilla* multibeam processing packages. *Livedata* performs bandpass estimation and removal, Doppler corrects the data, and calibrates the resulting spectrum (Barnes et al. 2001). The packages were modified by one of us (M.C.) to read Arecibo data, and new routines to reject RFI were implemented. Current versions of the *Livedata*/*Gridzilla* packages include these routines and are available at http://www.atnf.csiro.au/computing/

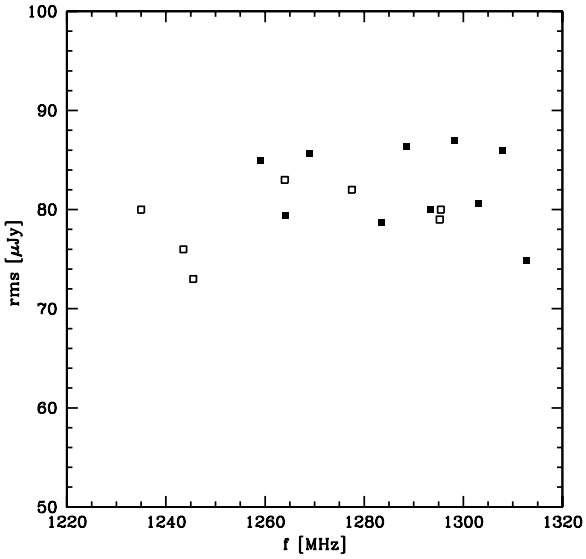


Figure 3. Measured rms in unsmoothed spectra with exposure times longer than 13.5 hr. All measurements were performed in parts of the spectra without line emission or RFI. Solid squares are measurements on extracted galaxy spectra close to the detected H I lines, whereas open squares are measurements at the center of the field.

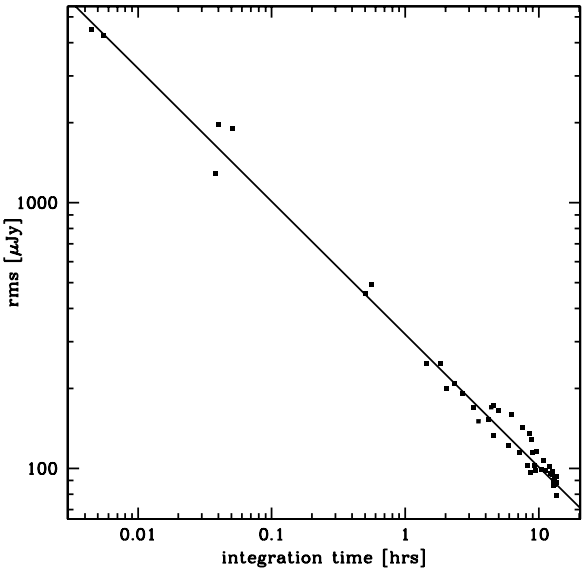


Figure 4. Measured rms at 1370 MHz in unsmoothed spectra along the central strip of the survey as a function of the total accumulated integration time. The line is a fit to the data of $\sigma \propto \sqrt{1/t_{\rm int}}$.

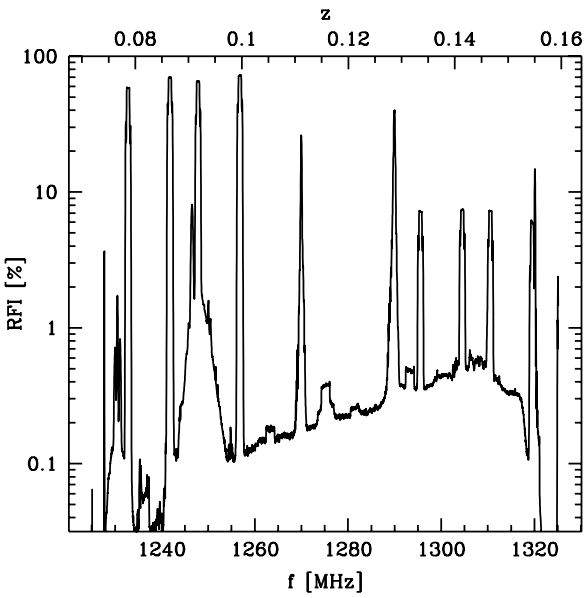


Figure 5. RFI occupancy versus frequency.

software/livedata.html. The bandpass was calculated independently for each drift, beam, and polarization. A clipped median was used to compute a reliable calibration factor for each spectral channel in the presence of strong and persistent RFI.

After the bandpass calibration, data points with RFI were flagged, both with an automatic procedure and manually (see below). Finally, flagged calibrated data were combined into a data cube using *Gridzilla*. For the precursor experiment, the array configuration was optimized to provide depth rather than uniform coverage, with the beams forming three independent strips separated in declination. In order to grid this efficiently, we chose a non-isotropic grid size, with pixels 1 arcmin in right ascension and 5.2 arcmin in declination. This gave one row of pixels for each strip. The cube was formed by median—combining the data from the calibrated spectra, weighted so as to correctly reconstruct the flux of a source at the pixel center. The final data cube had a size of 45 pixels in right ascension, three pixels in declination, and 4096 spectral channels.

2.5. RFI

All precursor data are impacted to some extent by RFI at various frequencies. In about 70% of all collected data, RFI was limited to well-known frequencies as listed in the observatory RFI catalog. In about 30% of the data, RFI at unusual frequencies occurred, sometimes wiping out large fractions of the bandpass. Our strategy for removing RFI was twofold. First, we implemented an automatic RFI removal routine based on 3.5σ clipping of the data smoothed in time–frequency space. Subsequently, we carefully edited out data sets with RFI not removed by our automatic procedure. The fraction of data rejected because of RFI as a function of frequency is shown in Figure 5. It can be seen that RFI appeared at all observed frequencies during the observations. About 6% of the band is severely affected by RFI with 10% or more of the data points being flagged. This corresponds to about 8% of the sampled volume affected heavily by RFI.

A concern for any deep survey is possible spurious detections of line emission caused by unrecognized RFI. Such a situation is most likely to happen close to spikes in the RFI spectrum. For example, the detected sources 2-4 and 2-6 are close to RFI spikes (see Section 3.1). We therefore re-examined this part of the spectrum and did not find any indication of undetected RFI. Later, we found that 2-6 was also detected in the SDSS at the exact redshift we determined from the H I observations. This confirms our ability to detect lines even in spectral regions close to RFI spikes.

3. RESULTS

3.1. Detection of H I Emitters

To search for H I emission lines in the final data cube, we created gray-scale plots of the flux density as a function of right ascension and frequency for each of the three strips. Each image was searched by eye for candidate H I emitters. Examples of two such candidates are shown in Figure 6. Individual scans for each candidate were carefully inspected to minimize the probability of including spurious RFI into the candidate list. We found 18 detected H I lines with a peak signal-to-noise ratio in the unsmoothed spectrum of at least 3, and a total width of the line of at least 20 spectral channels. Since the channels are mostly independent, the total signal-to-noise ratio of these lines is at least about $2\sigma \times \sqrt{20} \approx 9$.

We assigned a subjective quality code to each detected line, ranging from 1 for the best detections to 3 for detections that cannot be ruled out to be spurious. The criteria for the quality code were as follows. Isolated, high signal-to-noise ratio lines were assigned a quality code 1. Any line spectra for which the uncertainties in the baseline were judged to be a significant fraction of the detected line were assigned a quality code of 3. Spectral lines in this category have low signal-to-noise ratios, large variations in the baseline, and/or are uncomfortably close to RFI spikes. Spectra for which such an assignment was difficult to make were assigned the quality code 2. We suspect that several of the detected lines of the lowest quality are spurious, but note that the redshifts of two of them (AUDS 2-4 and 3-1) were later confirmed by optical redshift measurements in the SDSS.

For each detected line source, we extracted a total spectrum by summing up all adjacent spectra where flux at the corresponding redshift was detected with at least 3σ significance. The right

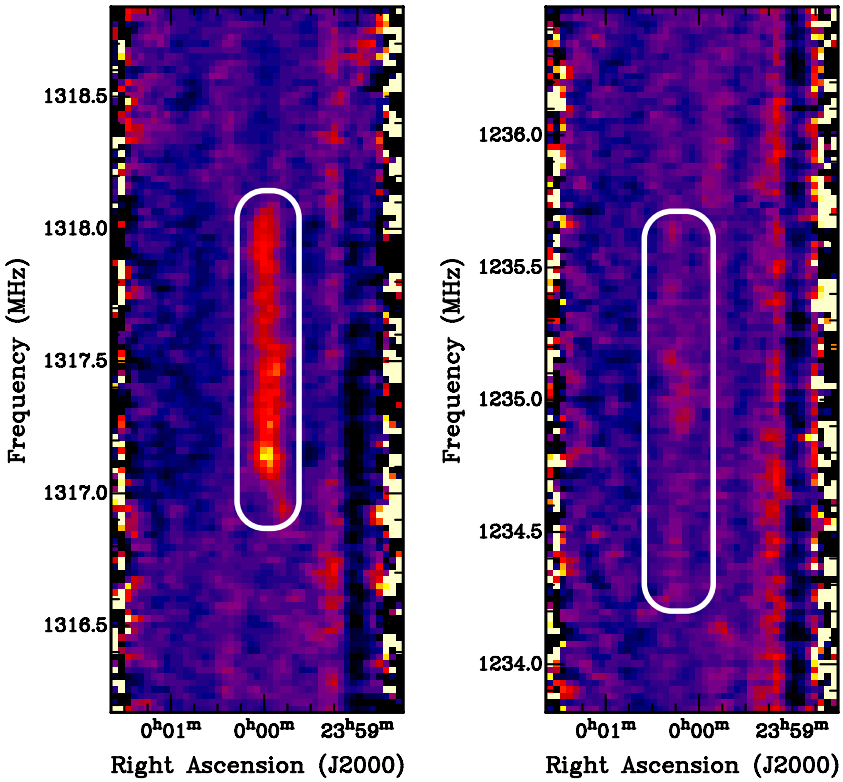


Figure 6. Examples of frequency–right ascension images used to search for H I emission. The two images are gray-scale plots around a high signal-to-noise ratio source (AUDS 2-3, left) and low signal-to-noise ratio source (AUDS 2-4, right). The detected lines are encircled in each image.
(A color version of this figure is available in the online journal.)

ascension of the source was computed at the center of flux from the positions with line emission. The extracted spectra for all 18 detections sorted by increasing right ascension are shown in Figure 7. Each detected source is named *s*–*n*, where *s* is the number of the strip 1, 2 or 3, and *n* is a running number within the strip in order of increasing right ascension. Figure 2 shows the distribution of the sources on the sky. Each source is marked by an ellipse which indicates the uncertainty in the position for high signal-to-noise sources. The positional uncertainty is discussed in more detail in the Appendix.

3.2. Analysis of Extracted Spectra

Frequencies were converted to velocities using standard relations (e.g., Greisen et al. 2006), and H I line parameters were estimated using the MBSPECT routine in the MIRIAD package (Sault et al. 1995) on the spectra after applying a 15 channel Hanning smoothing. Errors were estimated as in Koribalski et al. (2004). The measured parameters are listed in Table 2. The total H I content was estimated from the integrated line flux using the standard relation

$$M_{\rm H\,I} = 2.356 \times 10^5 \, \frac{M_\odot}{1+z} \, \frac{d_{\rm lum}^2}{\rm Mpc^2} \int \frac{I}{\rm Jy} \, \frac{dv}{(\rm km\,s^{-1})}, \quad (1)$$

where $d_{\rm lum}$ is the luminosity distance, and v is the measured optical velocity.

The AUDS precursor geometry of three strips along constant declination leads to a substantial positional uncertainty for the detected galaxies which will not be present in the better sampled full survey. The sensitivity between two strips is only a few percent compared to the center of a strip, and the strips are largely independent. We estimate the listed right ascension to be accurate to about 1/5th the HPBW of the beam, i.e., about 40 arcsec for high signal-to-noise detections in the central part of each strip. The position in declination is much less accurate, galaxies with large H I masses can be detected even if they are located between the strips. In the Appendix, the positional accuracy is discussed in more detail. Our inability to locate the galaxies precisely causes a bias in the mass estimate which does not exist in better sampled maps. Since the center of the beam is more sensitive than positions toward the edge, the positional uncertainty also leads to an uncertainty in the measured flux. H I masses computed using the gain for the center of the beam are therefore in most cases an underestimate of the true mass. We estimated the bias from this effect by using a Gaussian approximation for the shape of the ALFA beams (Irwin et al. 2009) and the redshift of each detected source to compute the total H I mass corresponding to the detected signal as a function of declination, $M_{\rm H\,I}(\delta)$. We then used the H I mass function $\Phi(M_{\rm H\,I})$ by Zwaan et al. (2003) to derive the probability $P(\delta)$ that the detected source is at that position:

$$P(\delta) = \frac{\Phi(M_{\rm H\,I}(\delta))}{\int_{-\pi/2}^{\pi/2} \Phi(M_{\rm H\,I}(\delta)) d\delta}. \quad (2)$$

Finally, we computed the expected H I mass as

$$M_{\rm H\,I}^{\rm corr} = \int M_{\rm H\,I}(\delta) P(\delta) d\delta. \quad (3)$$

The corrected H I masses range from 2 to 11 $\times$ 10^9 $M_\odot$, the detailed distribution is shown in Figure 8.

For six sources in our sample, a unique optical counterpart has been found (see Section 3.3). For those sources, the accuracy

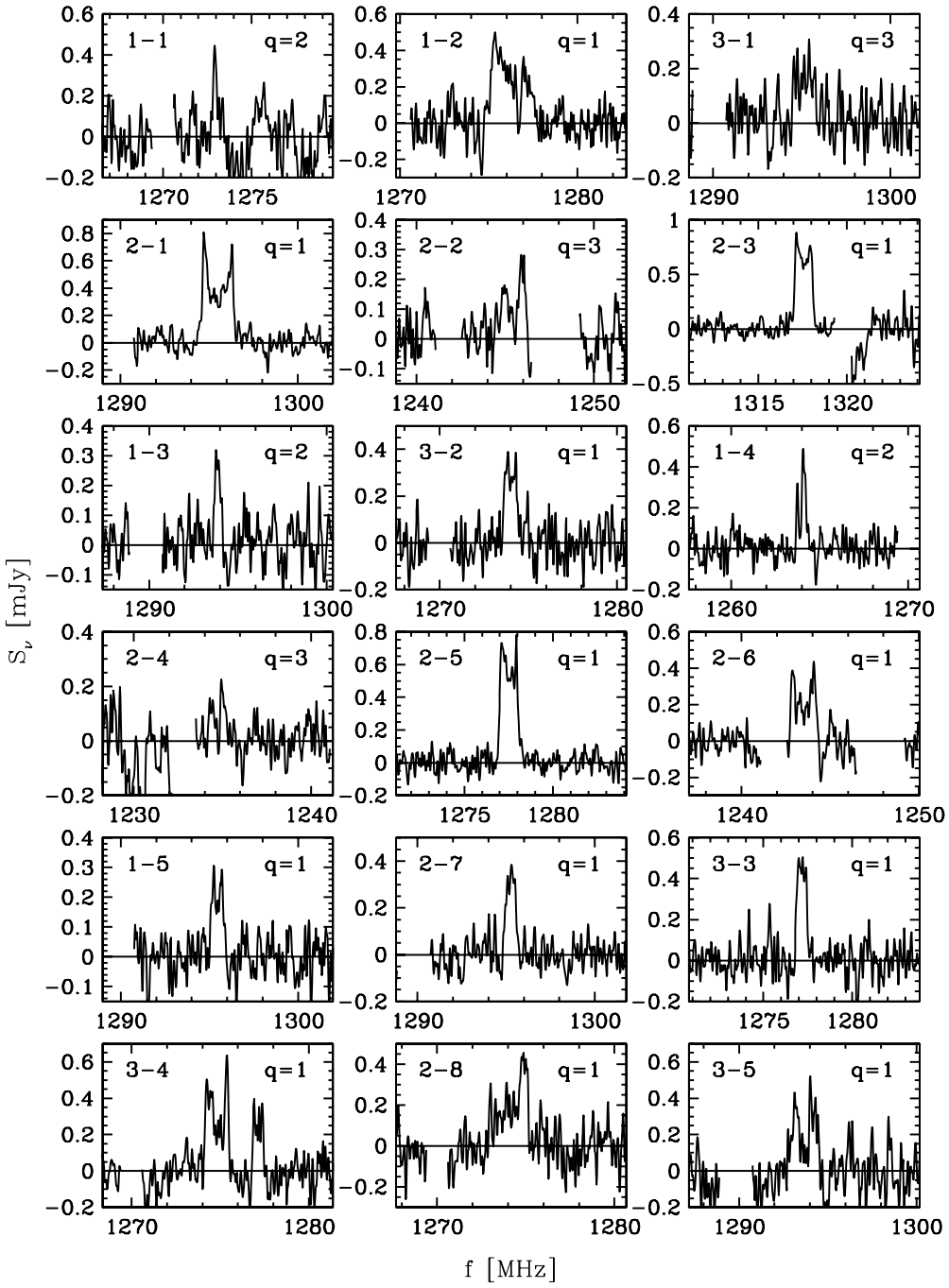


Figure 7. Spectra of all 18 H I emission lines detected in the AUDS precursor survey. A three channel Hanning smoothing and subsequent three channel boxcar smoothing have been applied to each raw spectrum. Regions where RFI was present more than 5% of the time are not plotted because of the high probability residuals from removed RFI. Each panel is labeled with the name of the source *n–m* and the quality code, which ranges from 1 for the best spectra to 3 for the lowest quality spectra.

of the bias correction can be independently checked. One of the sources, AUDS 3-1, is at a position about 2.6 arcmin from the center of the strip. At this position, the sensitivity of individual beams is only about 10%, but the effective beam shape of the drift scans is highly uncertain. Our model predicts that the probability that the detected galaxy is located that far from the center of the beam is less than 1%. The other five optical counterparts are on average at a distance of 0.66 arcmin from the center of their strip, and the average flux correction relative to the center of the strip is a factor of 1.15. Our bias model predicts an average most likely distance from strip center of 0.65, and an average correction factor of 1.20. We therefore conclude that our flux correction significantly reduces the biases in the mass estimate based on the sensitivity at the center of each strip.

The measured and derived H I parameters are listed in Table 2. The first line for each galaxy lists the measurements, and the second line gives the 1σ error estimates for each parameter. In detail, the individual columns contain the following: (1) assigned name in the form *n–m*, where *n* is the number of the declination strip and *m* is the running number assigned to each galaxy in order of increasing right ascension; (2) and (3) coordinates of the detected source; (4) measured noise in the unsmoothed spectrum close to the detected line; (5) peak signal-to-noise ratio of the unsmoothed line spectrum;

Table 2
Properties of AUDS Galaxies

ID	α_{2000}	δ_{2000}	rms (μJy)	S/N	q[a]	ν (MHz)	v_{50} (km s^{-1})	z	$d_{\rm lum}$ (Mpc)	w_{20} (km s^{-1})	$\int f dv$ (mJy·km s^{-1})	$M_{\rm H\,I}$ (10^9 $M_\odot$)	$M_{\rm H\,I,corr}$ (10^9 $M_\odot$)
(1)	(2)	(3)	(4)	(5)	(6)	(7)	(8)	(9)	(10)	(11)	(12)	(13)	(14)
1-1	23 59 18.3	15 37 28	152	3.5	2	1272.9	34728	0.11584	525.7	197	46	2.66	3.89
						0.8	22	0.00007	0.3	66	16	0.94	1.37
1-2	23 59 22.4	15 37 28	125	4.6	1	1276.1	33899	0.11308	512.2	662	160	8.88	10.02[b]
						0.8	21	0.00007	0.3	62	29	1.58	1.91
3-1	23 59 39.0	15 47 52	100	3.9	3	1295.1	28997	0.09672	433.2	346	43	1.73	8.97[b]
						0.6	14	0.00005	0.2	43	20	0.80	1.29
2-1	23 59 47.3	15 42 40	80	10.8	1	1295.5	28910	0.09643	431.8	480	189	7.58	7.59[b]
						0.3	7	0.00002	0.1	21	27	1.07	1.30
2-2	23 59 51.5	15 42 40	73	5.4	3	1245.5	42099	0.14043	647.9	497	62	5.37	6.88
						0.8	28	0.00009	0.4	85	20	1.70	2.18
2-3	23 59 59.8	15 42 40	167	5.9	1	1317.5	23408	0.07808	345.1	277	158	4.11	5.52
						0.3	6	0.00002	0.1	18	24	0.62	0.84
1-3	00 00 08.1	15 37 28	93	4.1	2	1293.9	29322	0.09781	438.3	127	24	0.99	1.83
						0.6	14	0.00005	0.2	41	11	0.46	0.86
3-2	00 00 08.1	15 47 52	105	5.1	1	1274.0	34452	0.11492	521.2	263	65	3.72	5.08
						0.5	14	0.00005	0.2	41	16	0.91	1.24
1-4	00 00 12.3	15 37 28	83	6.8	2	1264.0	37100	0.12375	564.6	189	46	3.06	4.35
						0.3	9	0.00003	0.1	26	11	0.74	1.06
2-4	00 00 12.3	15 42 40	80	3.5	3	1235.0	45011	0.15014	697.2	448	74	7.34	7.71[b]
						0.5	17	0.00006	0.3	52	22	2.21	2.71
2-5	00 00 16.4	15 42 40	82	10.4	1	1277.5	33533	0.11185	506.2	313	162	8.82	11.12[b]
						0.2	6	0.00002	0.1	18	19	1.04	1.25
2-6	00 00 16.4	15 42 40	76	6.2	1	1243.5	42645	0.14225	657.1	446	123	10.93	14.18[b]
						0.3	10	0.00003	0.2	30	23	2.05	2.43
1-5	00 00 20.6	15 37 28	89	3.8	1	1295.4	28922	0.09647	432.0	218	35	1.42	2.39
						0.7	15	0.00005	0.2	45	14	0.55	0.93
2-7	00 00 28.9	15 42 40	79	5.9	1	1295.2	28971	0.09664	432.7	205	53	2.13	3.26
						0.5	10	0.00003	0.2	31	13	0.51	0.79
3-3	00 00 33.0	15 47 52	111	5.2	1	1277.2	33626	0.11216	507.7	194	79	4.31	5.74
						0.3	7	0.00002	0.1	21	15	0.81	1.08
3-4	00 00 41.4	15 47 52	128	5.3	1	1274.8	34235	0.11420	517.7	365	102	5.79	7.34
						0.3	7	0.00002	0.1	22	22	1.23	1.56
3-5	00 00 49.7	15 47 52	138	4.4	1	1293.7	29354	0.09791	438.9	455	102	4.20	5.61
						0.7	16	0.00005	0.2	49	22	0.89	1.20
2-8	00 00 58.0	15 42 40	127	4.6	1	1274.0	34440	0.11488	521.0	593	117	6.68	8.31
						0.3	9	0.00003	0.1	27	25	1.42	1.76

Notes.
[a] Quality code for detection: 1, likely detection; 2, possible detection; 3, doubtful detection.
[b] Based on the position of the SDSS source.

(6) a quality code: 1—best detection; 2—likely detection but possibly affected by RFI; 3—uncertain detection because of low noise or RFI; (7) center frequency of line; (8) optical heliocentric velocity centroid, i.e., $c \cdot z$, measured at 50% of peak flux; (9) redshift z; (10) luminosity distances using $H_0 = 72$ km s^{-1} Mpc^{-1}, $\Omega_m = 0.26$, and $\Omega_\lambda = 0.74$.; (11) velocity width of line measured at 20% of the peak flux; (12) integrated line flux; (13) raw H I mass estimate; (14) H I mass estimate corrected for position bias. For sources 1-2, 2-1, 2-4, 2-5, 2-6, and 3-1, Column 14 lists the mass computed assuming the source position is identical to that of its SDSS counterpart.

3.3. Redshift Distribution and SDSS Identifications

The redshifts of the detected galaxies range from 0.07 to 0.15, see Figure 9 for the redshift distribution. Nine of the detected galaxies plus six more candidates are at a redshift above 0.1. This sample of at least nine H I rich galaxies at $z > 0.1$ is one of the largest field samples of H I sources at that redshift range.

Figure 2 shows the position and redshifts of the AUDS precursor sources, and also shows all spectroscopic sources with redshifts in the SDSS DR7 (Abazajian et al. 2009).

The six H I detections labeled 1-1, 2-1, 2-4, 2-5 and 2-6, which overlap in position, and 3-1 all have SDSS counterparts that match both in position and redshift. In order to search for plausible candidate galaxies for detections without matching redshifts in the SDSS, we carefully searched the beam area around each detection for optical galaxies in the SDSS. The details of the search are given in the Appendix, where we present images obtained with the SDSS finding chart tool at http://cas.sdss.org/dr7/en/tools/chart/chart.asp for each source. Plausible candidates for the H I emission are marked. At least one possible counterpart was found for each of the H I detections.

To investigate whether the sizes of the identified candidates make them plausible sources for the H I emission, we plotted the r-band isophotal major axes as listed in the SDSS as a function of redshift (Figure 10) and estimated H I mass (Figure 11). For H I detections without confirmed SDSS redshift, we used the major axis of the largest of the candidates. Figure 10 shows

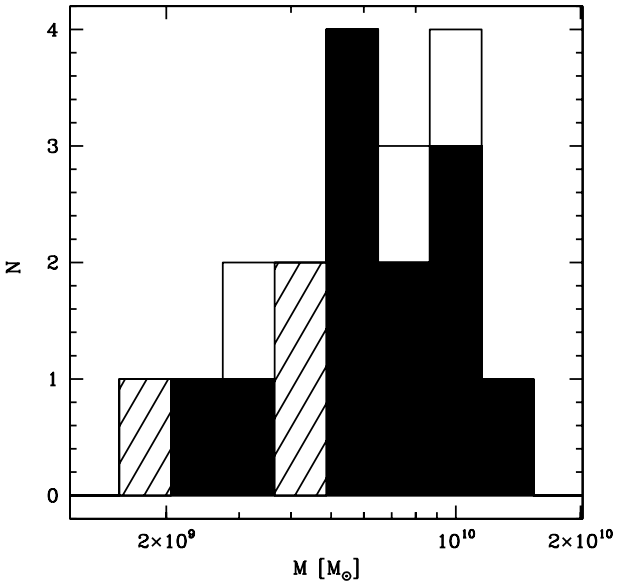


Figure 8. Mass distribution of H I lines detected in the AUDS precursor run. The filled parts of the histogram are the highest quality spectra, the shaded part is the medium quality, and the open parts are the lowest quality spectra.

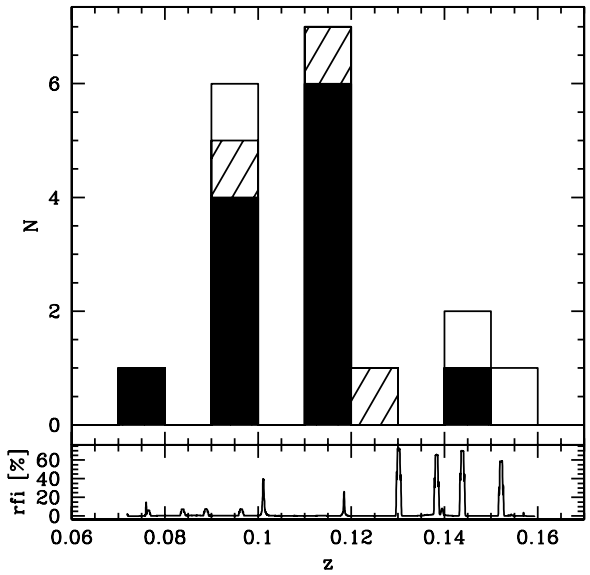


Figure 9. Redshift distribution of H I lines detected in the AUDS precursor run. The filled parts of the histogram are the highest quality spectra, the shaded part is the medium quality, and the open parts are the lowest quality spectra. For comparison, the RFI occupancy shown in Figure 5 is replotted in the lower panel.

that for all H I detections there are candidates with sizes similar to other SDSS galaxies at that redshift. Figure 11 shows that most candidates with unknown optical redshift are smaller than the redshift confirmed SDSS counterpart. These smaller sizes are plausible given the smaller H I masses of the unconfirmed candidates. We therefore conclude that for all our H I detections, plausible counterparts exist in the SDSS.

3.4. Detection Rate

The survey samples a rather small volume. The total volume within the area covered within the half-power sensitivity of at least one feed in each scan and between a redshift of 0.07 and 0.16 excluding regions heavily affected by RFI is about 2000 Mpc^3. The number of galaxies detected in such a volume will vary substantially for independent volumes simply due to

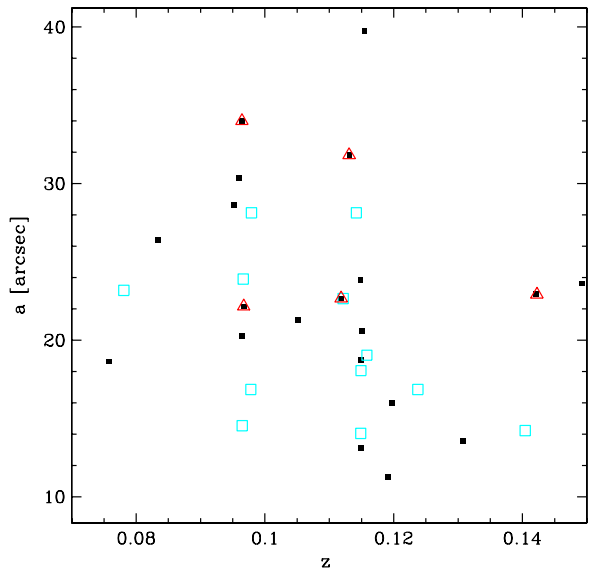


Figure 10. Distribution of *r*-band isophotal major axes vs. the redshift of H I and SDSS sources within the target region. Open triangles are the H I sources with SDSS counterparts confirmed by redshift, open squares those without such confirmation, and solid squares are SDSS galaxies in the AUDS precursor region. For sources without counterparts confirmed by redshift, the major axis of the largest plausible candidate in the field was used.

(A color version of this figure is available in the online journal.)

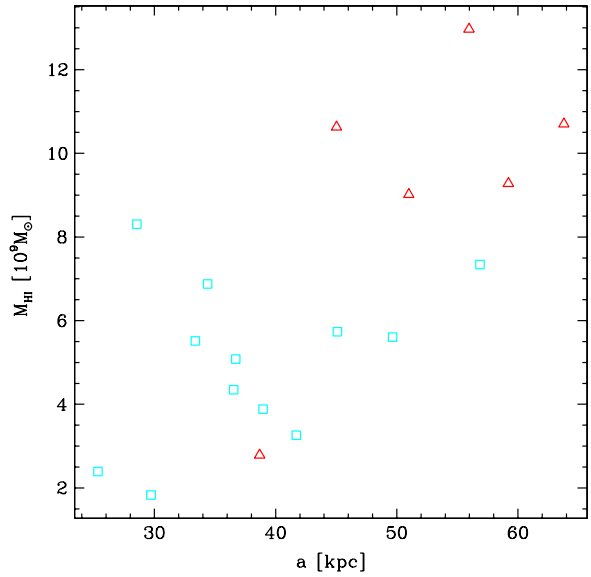


Figure 11. Scatter plot of the estimated H I masses vs. the *r*-band isophotal major axes. Open triangles are the H I sources with SDSS counterparts confirmed by redshift, and open squares represent those without such confirmation. For sources without counterparts confirmed by redshift, the major axis of the largest plausible candidate in the field was used to compute the rest-frame size.

(A color version of this figure is available in the online journal.)

cosmic variance. We estimated the expected cosmic variance of the number counts in this volume from the catalog of Croton et al. (2006). The H I mass function recovered from this catalog resembles the one of Zwaan et al. (2003). We extracted 1000 mock surveys of galaxies with the same sensitivity and volume shape as the real data. We found that the 1σ variation of the mean number of galaxies in the mock survey scatter is about 50%.

In addition, the selected volume is not a fair sample of that redshift range because it was not chosen at random.

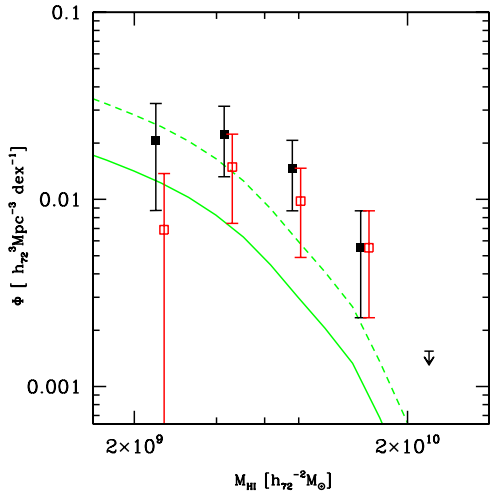


Figure 12. H I mass function of detected H I emitters. Filled squares are the points derived using all detected H I emitters, whereas the open squares only use the highest quality detection. The solid line is the local H I mass function by Zwaan et al. (2005). The dashed line is the local H I mass function multiplied by the relative overdensity of SDSS galaxies within the survey region (see the text). The arrow marks the resulting density if a single galaxy had been detected in that bin.

(A color version of this figure is available in the online journal.)

Nevertheless, it is illustrative to compare the detection rate of galaxies to that expected from the local H I mass function.

For that purpose, we computed the H I mass function from our sample using the standard $1/v_{\rm max}$ method (Schmidt 1968). Volumes were computed using the same Gaussian approximation for the shape of the beam as in Section 3.2. For comparison, we also estimated the H I mass function assuming a distribution function for the H I flux and line width. The results were similar to the ones shown here. The result with the $1/v_{\rm max}$ method using the full sample is shown as filled squares in Figure 12. The local H I mass function determined from the HIPASS survey (Zwaan et al. 2005) is shown as a solid line. It can be seen that the shape of the derived mass function is consistent with the HIPASS H I mass function. We used a weighted fit to determine that the relative normalizations between the two H I mass functions differ by a factor of 3.2 ± 1.0. We then recomputed the H I mass function after removing detections with the lowest quality rating. The normalization of the derived H I mass function from this reduced sample is still a factor of 2.1 ± 0.7 higher than the local H I mass function. We adopt the mean of the two factors and the mean relative error, $\delta_{\rm H\,I} = 2.6 \pm 0.8$, as our best estimate of the relative H I overdensity in the AUDS precursor region and its uncertainty.

For comparison, we estimated the relative density of SDSS galaxies within the AUDS precursor survey volume. For that purpose, we extracted the SDSS photometric redshifts for galaxies with *r*-band isophotal major axes between 5 and 40 arcsec. The selection on the major axes was imposed to eliminate galaxies with implausible photometric redshifts from the sample. The limits were chosen to include all candidate SDSS counterparts, see Section 3.3 and Figure 10. The results presented below are insensitive to the exact range of selected isophotal major axes. There are 55 galaxies selected in that manner within the AUDS precursor survey volume.

We tested the success of our selection procedure for the subsample of galaxies with available spectroscopic redshifts. We found that all galaxies that are within the AUDS redshift range based on their spectroscopic redshift are also correctly placed within that volume by their photometric redshift. There is only one galaxy which is placed within that volume by its photometric redshift even though the spectroscopic redshift is outside that range. The spectroscopic redshift of that galaxy is 0.1502. We therefore conclude that the SDSS photometric redshifts are accurate enough to estimate the relative densities of volumes in the AUDS redshift range.

We then counted the number of galaxies selected in the same manner in 100 close-by regions of the same size and shape. We find that on average, there are 22.3 ± 1.3 galaxies in regions of that size, where 1.3 is the uncertainty of the mean based on the scatter in the number counts. The overdensity of SDSS galaxies in the AUDS precursor region is therefore about $\delta_{\rm SDSS} = 2.5 \pm 0.4$, where the error estimate includes the Poisson error on the number counts within the AUDS volume. Assuming that the ratio between H I density and that of SDSS galaxies is independent of the local overdensity, we can estimate the mean H I density at median redshift of the AUDS precursor survey in terms of the H I density at zero redshift ρ_0 to be

$$\rho_{\rm H\,I}(z = 0.125) = \frac{\delta_{\rm H\,I}}{\delta_{\rm SDSS}} \rho_0 = (1.0 \pm 0.3) \cdot \rho_0. \qquad (4)$$

The error estimate includes only random errors. When we use the SDSS spectroscopic redshifts to estimate the relative overdensity in the same manner as above, the result is $\rho_{\rm H\,I}(z = 0.125) = (1.3 \pm 0.6) \cdot \rho_0$. The larger uncertainty is due to the smaller number of galaxies with measured spectroscopic redshift.

4. SUMMARY AND CONCLUSION

We have used about 53 hr of integration time with the Arecibo telescope to demonstrate the feasibility of high sensitivity H I observations with the Arecibo *L*-band Feed Array. To this depth, the noise in the final spectra still behaves as $\propto \sqrt{1/t_{\rm exp}}$. RFI renders a significant fraction of the spectrum useless. However, regions of the spectrum where RFI is rarely present are little affected by the strong RFI in neighboring channels.

In total, we detected 18 H I emitters in the survey. For six of them, there are optical counterparts with measured redshifts in the SDSS. For all other detections, there are plausible SDSS counterparts without redshift confirmation. The detection rate is consistent with the total H I density in the local universe.

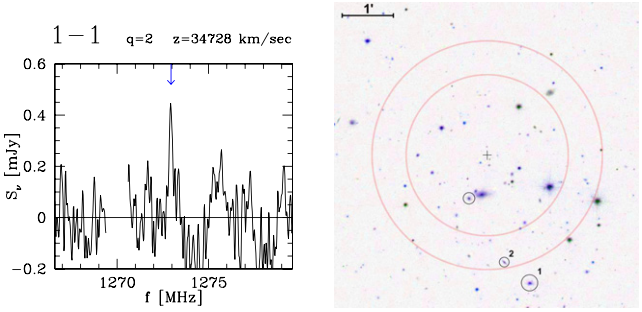
The experiment was a pilot study for the "AUDS." This survey will be more sensitive, cover more area on the sky with a better sampling, and probe a larger redshift range than this pilot study. AUDS will allow us to investigate in detail the H I content in two independent volumes outside the local universe.

This research has made use of the Sloan Digital Sky Survey archive. Its full acknowledgment can be found at http://www.sdss.org.

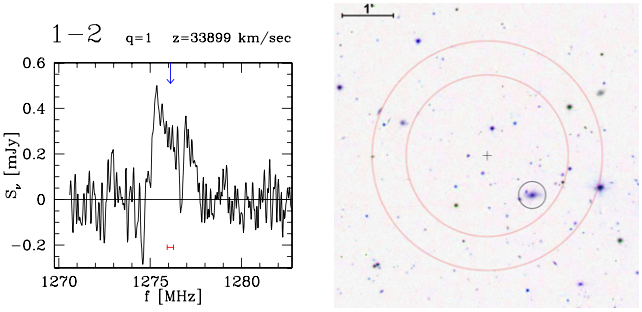
APPENDIX

SDSS COUNTERPARTS OF AUDS H I DETECTIONS

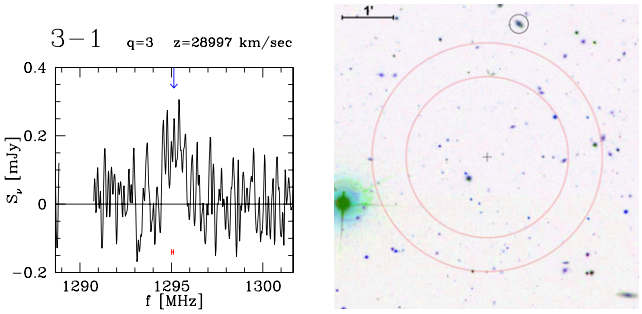
The target field for the AUDS precursor survey was chosen to include galaxies that were likely to be strong H I emitters as judged by the SDSS spectrum. Those galaxies were intentionally placed close to the center of the central strip in the most sensitive part of the survey. The H I counterparts for these galaxies can easily be identified by redshift. The final data cube of the survey



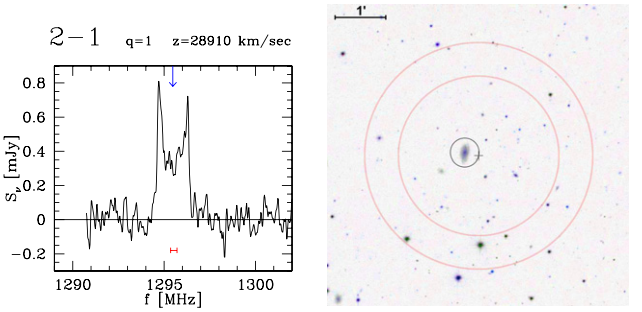
The narrow line width of 197 km s^{-1} suggests a relatively face-on galaxy. Because of the low signal-to-noise ratio, we cannot exclude a substantially larger line width. The H I line is also visible in the spectrum of source 1-2, which is consistent with the position of SDSS 235914.9+153457. Source 1-2 is within the beam, and its line is visible in the spectrum between 1275 and 1279 MHz.



The redshift of SDSS 255918.8+153641 is marked in the H I spectrum. Source 1-1 is also in the beam and its line is visible at around 1272 MHz.

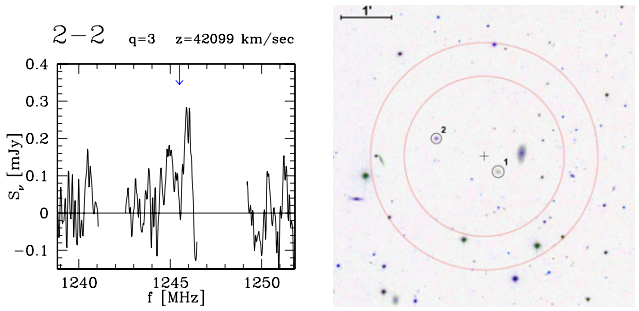


The redshift of SDSS 235936.4+155029 is marked in the spectrum. It is located close to the edge of the image cutout, where the sensitivity is about 10% of the sensitivity at the center of the beam. The relatively low H I mass estimate of $1.7 \times 10^9\ M_\odot$ is consistent with such an off-center position.

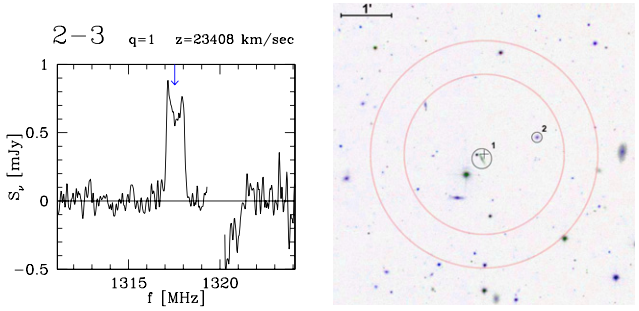


SDSS 235948.4+154243 was one of the sources used to select the target region. Its SDSS redshift is marked in the spectrum.

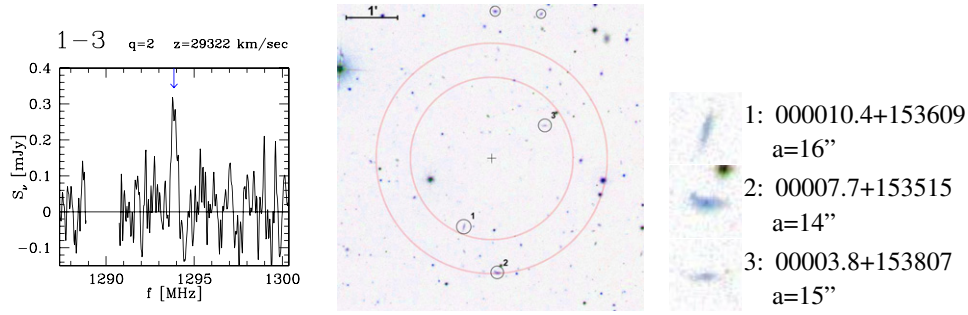
Figure A1. Figure A1. SDSS counterparts.
(A color version of this figure is available in the online journal.)



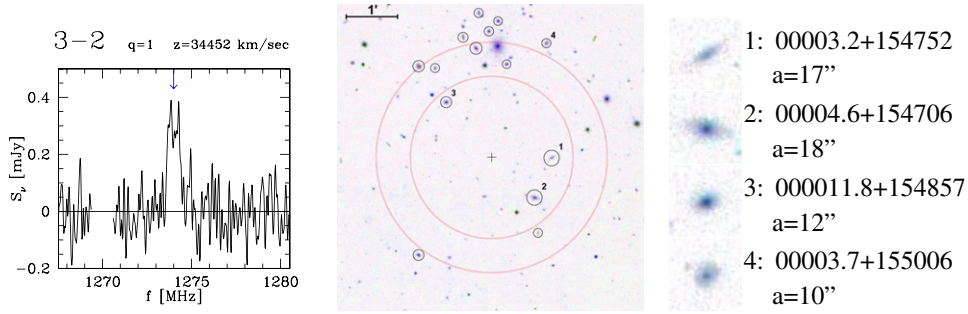
HI emission is between regions with frequent RFI. Both candidate SDSS counterparts are low surface brightness galaxies.



The line width of 277 $\mathrm{km\,s^{-1}}$ suggests a highly inclined galaxy. This makes SDSS 235960.0+154235 the most likely optical counterpart.

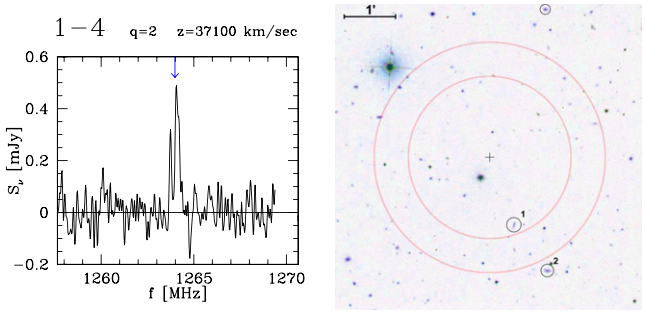


The narrow line width suggest a relatively face-on galaxy, whereas the SDSS counterparts are fairly inclined disks. Because of the low signal-to-noise ratio, the line width could be underestimated. The beam overlaps with the one of source 1-4, and they share two of the candidate counterparts.

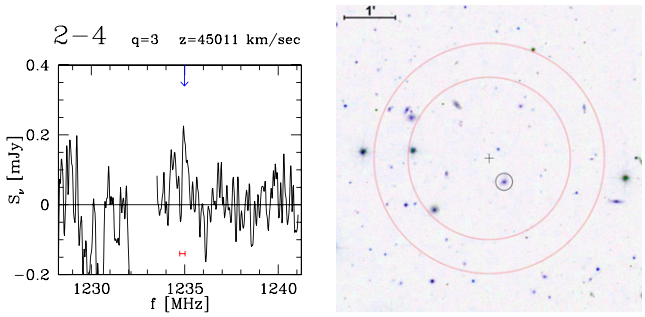


A cluster at $z \approx 0.152$ to the north of the beam was not detected. Only one of the cluster members has a measured optical redshift. It is therefore possible that one of the apparent cluster members is the optical counterpart of the HI emission.

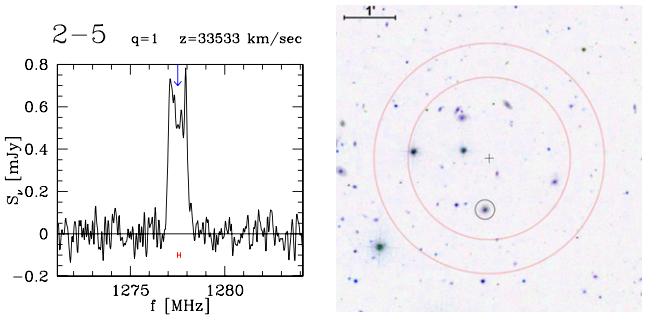
Figure A1. (Continued)



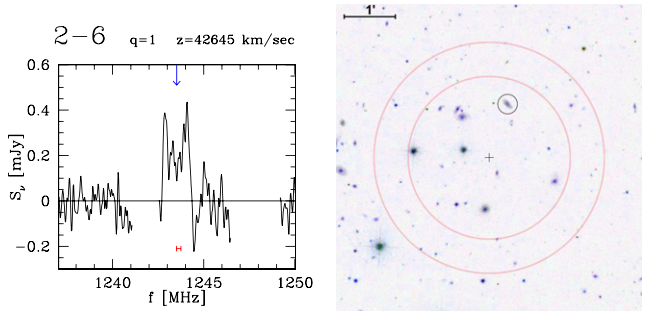
The narrow line width suggest a relatively face-on galaxy, whereas the SDSS counterparts are fairly inclined disks. The beam overlaps with the one of source 1-3.



Because of the low signal-to-noise ratio and the closeness of a region with frequent RFI, the quality of the spectrum was judged to be low. However, the exact match in redshift confirms the reality of the detected line. The redshift of SDSS 000011.1+154212 is marked in the spectrum.

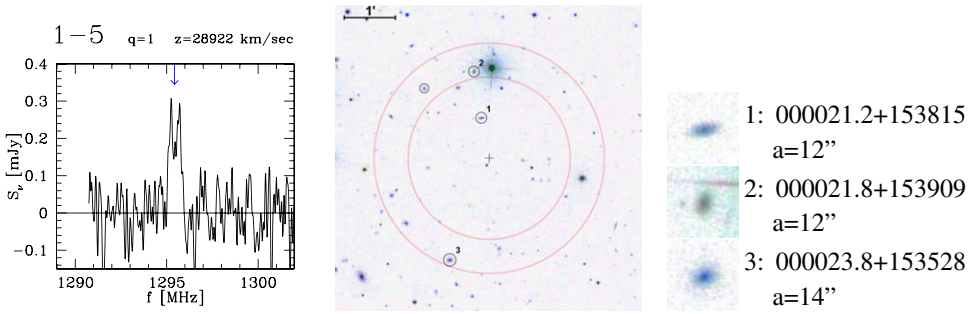


SDSS 000016.8+154140 was one of the sources used to select the target region. Its SDSS redshift is marked in the spectrum. The measured position of source 2-5 is identical to source 2-6.

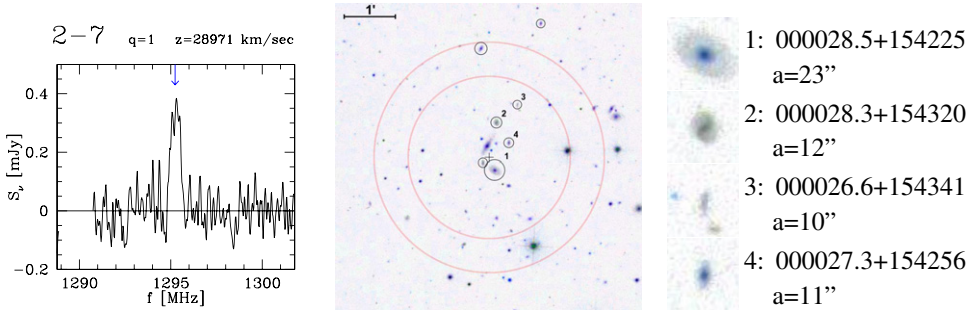


SDSS 000014.9+154342 was one of the sources used to select the target region. Its SDSS redshift is marked in the spectrum. The measured position of source 2-6 is identical to source 2-5. The line is close to a region in the spectrum with well known RFI at Arecibo. We used this fact to test our ability to detect lines close to RFI.

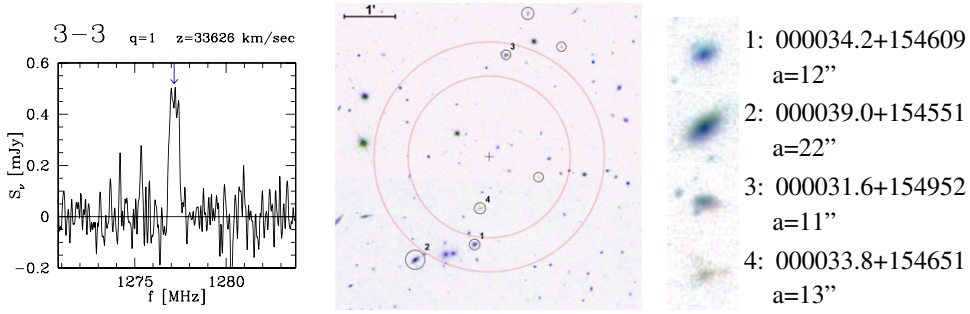
Figure A1. (Continued)



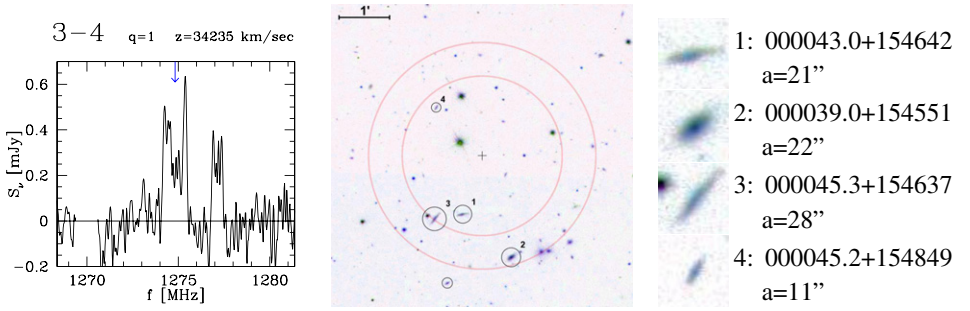
Because of its high signal-to-noise ratio, the positional uncertainty in right ascension should be small. Another potential counterpart is partially hidden by the bright star close to 000021.8+153909. It is not marked because the SDSS measurement of the major axis is not reliable.



The edge-on disk galaxy at the center of this beam is at a redshift of 0.115 and was not detected.

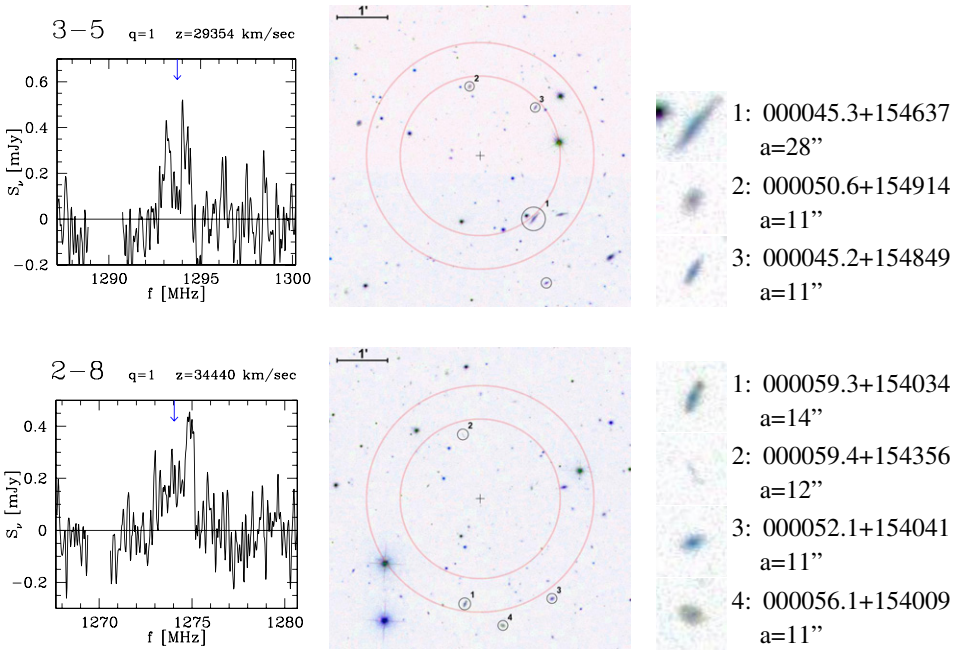


SDSS 000039.0+154551 is probably too far off-center to be the optical counterpart given the high signal-to-noise ratio of the detected HI line. The peaks of the double-horned profile of source 3-4 are visible in the spectrum at ≈ 1274 and 1275.5 MHz.



The beam overlaps with the ones around sources 3-5 and 3-3. The second line in the spectrum centered at ≈ 1277 MHz originates from source 3-3.

Figure A1. (Continued)



The high line width of 593 km s^{-1} suggests a highly inclined galaxy. For that reason, 000059.3+154034 is the most likely optical counterpart.

Figure A1. (Continued)

was searched for H I detections without knowledge of the location or redshift of SDSS galaxies in this volume. Most of the H I detections are lower in the H I content than the preselected targets, and most of them are without matching the redshift listed in the SDSS. Identifying the optical counterparts for those sources is difficult because of the large beam size.

Because of the geometry of the survey, the declination of a source is very uncertain. The sensitivity of the telescope beam between the strips drops to about 10% of the sensitivity at the center of the strips. A strong source can therefore be detected at any position within the survey region, including the region between the strips. If a source is located at a large angular distance from the center of the strip, the measurement error in right ascension becomes dominated by the lack of our knowledge of the exact beam shape. The ALFA beam shape at a larger distance from the center varies strongly with the pointing of the telescope (Irwin et al. 2009), and the effective beam shape of our repeated drifts is highly uncertain. An accurate estimate of the positional uncertainties as a function of signal-to-noise ratio is therefore difficult. For simplicity, we adopt 20% of the FWHM beam as our estimated uncertainty in right ascension for all of our sources.

We searched for optical counterparts within 3.2 arcmin of the H I position in right ascension and 6 arcmin in declination. This corresponds to a sensitivity of 50% and 10% of that at the center of the beam. Within that region, we selected possible optical counterparts from the SDSS that were classified as galaxies and had a major axis of 10 arcsec or more in the SDSS *r* band. We manually cleaned the extracted source list by inspecting their images and removing misidentification such as double stars or image defects. If the SDSS redshift of any of the candidates was within the detected H I line, we adopted this source as a certain detection of a unique optical counterpart.

In Figure A1, we show a region of 6 × 6 arcmin^2 around each AUDS source obtained from the SDSS finding chart generator. For better clarity, the images are shown with inverted color scale, i.e., bluer colors represent redder galaxies. The sensitivity at the edges of the images is approximately 10% of the sensitivity at the center. In each image, the approximate size of the beam at 50% and 25% of the beam center is marked as circles. The outer part of the shown region corresponds to about 10% the sensitivity of the center of the beam. For sources with a unique optical counterpart, the counterpart galaxy is circled. For all other sources, all possible counterparts are marked with circles. The diameter of each circle is the size of the major axis of each source as listed in the SDSS. For each source, we selected up to four candidates we judged to be the most likely optical counterparts based on the following criteria: (1) counterparts are more likely to be located close to the center of the field, (2) H I line widths larger than 400 km s^{-1} are likely to correspond to galaxies with highly inclined disks, whereas those smaller than 200 km s^{-1} should correspond to almost face-on disks, and (3) larger sources are more likely to contain large amounts of H I. The most likely candidate counterpart galaxies are also shown separately in cutouts 20 × 20 arcsec in size, and their major axis *a* is given. For easy comparison, we also reproduce the H I spectrum for each source. In this spectrum, the measure H I redshift is marked by an arrow at the top, and if available, the SDSS redshift with error estimated is marked by a bar below the H I line.

REFERENCES

Abazajian, K. N., et al. 2004, AJ, 128, 502
Abazajian, K. N., et al. 2009, ApJS, 182, 543
Auld, R., et al. 2006, MNRAS, 371, 1617
Barnes, D. G., et al. 2001, MNRAS, 322, 486
Bouwens, R. J., Illingworth, G. D., Blakeslee, J. P., Broadhurst, T. J., & Franx, M. 2004, ApJ, 611, L1
Catinella, B., Haynes, M. P., Giovanelli, R., Gardner, J. P., & Connolly, A. J. 2008, ApJ, 685, L13
Croton, D. J., et al. 2006, MNRAS, 365, 11
Daddi, E., Dannerbauer, H., Elbaz, D., Dickinson, M., Morrison, G., Stern, D., & Ravindranath, S. 2008, ApJ, 673, L21

Giovanelli, R., et al. 2005, AJ, 130, 2598
Giovanelli, R., et al. 2007, AJ, 133, 2569
Greisen, E. W., Calabretta, M. R., Valdes, F. G., & Allen, S. L. 2006, A&A, 446, 747
Haarsma, D. B., Partridge, R. B., Windhorst, R. A., & Richards, E. A. 2000, ApJ, 544, 641
Henning, P. A., et al. 2000, AJ, 119, 2686
Henning, P. A., et al. 2010, AJ, 139, 2130
Hopkins, A. M. 2004, ApJ, 615, 209
Irwin, J. A., et al. 2009, ApJ, 692, 1447
Koribalski, B. S., et al. 2004, AJ, 128, 16
Kovač, K., Oosterloo, T. A., & van der Hulst, J. M. 2009, MNRAS, 400, 743
Lah, P., et al. 2007, MNRAS, 376, 1357
Lah, P., et al. 2009, MNRAS, 399, 1447
Lang, R. H., et al. 2003, MNRAS, 342, 738
Madau, P., Ferguson, H. C., Dickinson, M. E., Giavalisco, M., Steidel, C. C., & Fruchter, A. 1996, MNRAS, 283, 1388
Meyer, M. J., et al. 2004, MNRAS, 350, 1195
Minchin, R. F., et al. 2003, MNRAS, 346, 787
Obreschkow, D., & Rawlings, S. 2009, ApJ, 696, L129
Pei, Y. C., Fall, S. M., & Hauser, M. G. 1999, ApJ, 522, 604
Popping, A., & Braun, R. 2007, New Astron. Rev., 51, 24
Power, C., Baugh, C. M., & Lacey, C. G. 2009, MNRAS, 406, 43
Prochaska, J. X., Chen, H.-W., Howk, J. C., Weiner, B. J., & Mulchaey, J. 2004, ApJ, 617, 718
Prochaska, J. X., Herbert-Fort, S., & Wolfe, A. M. 2005, ApJ, 635, 123
Rao, S. M., Prochaska, J. X., Howk, J. C., & Wolfe, A. M. 2005, AJ, 129, 9
Rivers, A. J., Henning, P. A., & Kraan-Korteweg, R. C. 1999, PASA, 16, 48
Rosenberg, J. L., & Schneider, S. E. 2000, ApJS, 130, 177
Rosenberg, J. L., & Schneider, S. E. 2003, ApJ, 585, 256
Ryan-Weber, E. V., Webster, R. L., & Staveley-Smith, L. 2003, MNRAS, 343, 1195
Sancisi, R., Fraternali, F., Oosterloo, T., & van der Hulst, T. 2008, A&AR, 15, 189
Sault, R. J., Teuben, P. J., & Wright, M. C. H. 1995, in ASP Conf. Ser. 77, Astronomical Data Analysis Software and Systems IV, ed. R. A. Shaw, H. E. Payne, & J. J. E. Hayes (San Francisco, CA: ASP), 433
Schmidt, M. 1968, ApJ, 151, 393
Spitzak, J. G., & Schneider, S. E. 1998, ApJS, 119, 159
Springob, C. M., Haynes, M. P., Giovanelli, R., & Kent, B. R. 2005, ApJS, 160, 149
Storrie-Lombardi, L. J., & Wolfe, A. M. 2000, ApJ, 543, 552
Verheijen, M., van Gorkom, J. H., Szomoru, A., Dwarakanath, K. S., Poggianti, B. M., & Schiminovich, D. 2007, ApJ, 668, L9
Winkel, B., Kerp, J., Kalberla, P. M. W., & Keller, R. 2008, in AIP Conf. Proc. 1035, The Evolution of Galaxies Through the Neutral Hydrogen Window, ed. R. Minchin & E. Momjian (Melville, NY: AIP), 259
Wong, O. I., et al. 2006, MNRAS, 371, 1855
Wong, T. 2009, ApJ, 705, 650
Zwaan, M. A., Briggs, F. H., Sprayberry, D., & Sorar, E. 1997, ApJ, 490, 173
Zwaan, M. A., Meyer, M. J., Staveley-Smith, L., & Webster, R. L. 2005, MNRAS, 359, L30
Zwaan, M. A., van Dokkum, P. G., & Verheijen, M. A. W. 2001, Science, 293, 1800
Zwaan, M. A., et al. 2003, AJ, 125, 2842